J Mater Sci (2010) 45:3259–3265
DOI 10.1007/s10853-010-4335-5

First-principles study on electronic properties of SiC nanoribbon

Jian-Min Zhang · Fang-Ling Zheng · Yan Zhang · Vincent Ji

Received: 28 December 2009 / Accepted: 18 February 2010 / Published online: 6 March 2010

Abstract Under the generalized gradient approximation (GGA), the electronic properties are studied for SiC nanoribbon with zigzag edge (ZSiCNR) and armchair edge (ASiCNR) by using the first-principles projector-augmented wave (PAW) potential within the density function theory (DFT) framework. Distinct variation behaviors in band gap are exhibited with increasing ribbon width. The ZSiCNR is metallic except for the thinner ribbons ($N_z = 2$–4) with small direct band gaps, while the direct band gaps of ASiCNR exhibit sawtooth-like periodic oscillation features and quench to a constant value of 2.359 eV as width N_a increases. The PDOS onto individual atom shows that a sharp peak appeared at the Fermi level for broader ZSiCNR comes from the edge C and Si atoms with H terminations. The charge density contours analysis shows the valence charges are strongly accumulated around C atom, reflecting a significant electron transfer from Si atom to C atom and thus an ionic binding feature. In addition, the Si–H bond is also ionic bond while the C–H bond is covalent bond. The dangling bonds give rise to one (two) flat extra band at the Fermi level for ZSiCNR with either bare C or bare Si edge (for ZSiCNR with bare C and Si edges as well as for ASiCNR with either bare C edge or bare Si edge), except for ASiCNR with bare C and Si edges in which two nearly flat extra bands appear up and below the Fermi level.

J.-M. Zhang (✉) · F.-L. Zheng
College of Physics and Information Technology, Shaanxi Normal University, Xian 710062, Shaanxi, People's Republic of China
e-mail: jianm_zhang@yahoo.com

Y. Zhang · V. Ji
ICMMO/LEMHE UMR CNRS 8182, Université Paris-Sud 11, 91405 Orsay Cedex, France

Introduction

During the last few decades, the graphene nanoribbon (GNR) attracted much attention due to their fascinating properties and potential application in nanoelectronics. Experimentally, the GNR has been prepared either by cutting mechanically exfoliated graphenes or patterning epitaxially grown graphenes [1–5]. Theoretically, the GNR with zigzag edge (ZGNR) possesses partly flat bands at the Fermi level and thereby gives a sharp peak in the density of states. The charge density in the edge state is strongly localized on the zigzag edge sites [6–8]. However, no such localized state appears in the GNR with armchair edge (AGNR). The energy band of AGNR is direct and the band gap depends on the width of the ribbon [9, 10].

It is well known that C and Si present completely different bonding characteristics, though they both are in the fourth column of the periodic table and have the same number of valence electrons. This happens because in carbon sp^2 hybridization is more stable while in silicon the preferable hybridization is sp^3. Thus, SiC bulk possesses unique physical and electronic properties which make it a suitable material for the fabrication of electronic devices for high-temperature, high-power, and high-frequency applications [11]. Furthermore, one-dimensional SiC nanosystems may exhibit unique properties due to quantum-size effects, making them useful materials in nanotechnology and nanoscale engineering. However, to our knowledge, the dependence of electronic properties on the width and chirality of SiC nanoribbon (SiCNR) are scarcely studied and are therefore highly desirable.

In this article, the SiC nanoribbon with zigzag edge (ZSiCNR) and armchair edge (ASiCNR) with and without H atoms terminated have been investigated by using the first-principles projector-augmented wave (PAW) potential

within the density function theory (DFT) framework under the generalized gradient approximation (GGA). The rest of the article is organized as follows. In the second section, the structure model and calculation methods are described in detail. The calculated results and discussions are given in the third section. The last section is devoted to the conclusions.

Structure model and calculation method

The hexagonal network of SiCNR consists of alternating Si and C atoms with each Si atom having three C atoms as its nearest neighbors and vice versa. H atoms are attached to the edge atoms to ensure that dangling bonds make no contribution to the electronic state near the Fermi level. Following the previous convention used for GNRs and BN nanoribbons (BNNRs) [12, 13], the width of ZSiCNR is classified by the number of the zigzag chains (N_z) across the ribbon width. Likewise, the width of ASiCNR is classified by the number of dimer lines (N_a) across the ribbon width. Thus, we refer a ZSiCNR with N_z chains as N_z-ZSiCNR and an ASiCNR with N_a dimer lines as N_a-ASiCNR. As examples, the geometry structures of the 6-ZSiCNR and 6-ASiCNR terminated with H atoms are shown in Fig. 1a and b. The area between two dashed lines represents the prime periodic unit cell in which there are six C and six Si atoms for either 6-ZSiCNR or 6-ASiCNR, but two H atoms for 6-ZSiCNR and four H atoms for 6-ASiCNR.

The calculations are performed using the Vienna ab initio simulation package (VASP) based on DFT [14–17]. For the mixing of the charge density an efficient Broyden/Pulay mixing scheme [18–20] is used. The electron-ionic core interaction is represented by PAW potentials [21] which are more accurate than the ultrasoft pseudopotentials. To treat electron exchange and correlation, we chose the Perdew–Burke–Ernzerhof (PBE) [22] formulation of the GGA, which yields the correct ground-state structure of the combined systems. A conjugate-gradient algorithm is used to relax the ions into their ground-states, and the energies and the forces on each ion are converged within 1.0×10^{-4} eV/atom and 0.02 eV/Å, respectively. The cutoff energy for the plane-waves is chosen to be 400 eV. The C $2s^2 2p^2$, Si $3s^2 3p^2$, and H $1s^1$ electrons are treated as valence electrons. The vacuum space is set to be 15 Å in both edge-to-edge and layer-to-layer directions, which is large enough to separate the interaction between SiCNR and its periodic images. The Brillouin zone integration is performed by using the Gamma-centered Monkhorst–Pack scheme [23] with $1 \times 1 \times 11$ k-points, together with a Gaussian smearing broadening of 0.2 eV. The accurate band structure calculations are preformed by using 60 k-points along the nanoribbon axis. After geometry optimization, we find the average Si–C bond length is 1.80 Å. This is in good agreement with previous calculations for SiC nanotubes (SiCNT) [24–26]. The C–H and the Si–H bond lengths are 1.10 and 1.49 Å, respectively. It is noted that these values are very close to the bond lengths in CH_4 (1.09 Å) and SiH_4 (1.49 Å). We know that the C–H and Si–H bond lengths for C atoms being hydrogenated and Si atoms being hydrogenated are 1.11 and 1.52 Å for SiCNT [27].

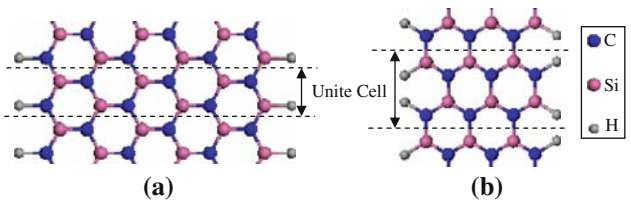

Fig. 1 The geometry structures of **a** 6-ZSiCNR and **b** 6-ASiCNR terminated with H atoms. The area between two *dashed lines* represents the prime periodic unit cell

Results and discussions

The typical band structures are shown in Fig. 2 for (a) 2-ZSiCNR, (b) 6-ZSiCNR, (c) 12-ZSiCNR, (d) 3-ASiCNR, (e) 6-ASiCNR, and (f) 12-ASiCNR as examples. For 6-ZSiCNR and 12-ZSiCNR, the lowest unoccupied conduction band (LUCB) and the highest occupied valence band (HOVB) meet at one k point near Z at the Fermi level and then separate from each other. This kind of edge state is different from the flat edge state at the Fermi level for ZGNR [6] but will also give rise to a remarkable sharp peak in the density of states (DOS) (see Fig. 4a). It is worth to note that the 2-ZSiCNR has a direct band gap of 0.975 eV. For 3-, 6-, and 12-ASiCNRs, the LUCB and the HOVB appeared at Γ point are always separated representing a direct semiconductor character. Furthermore, the band gap decreases for 3-, 6-, and 12-ASiCNRs successively. This is different from zigzag SiCNT constructed by rolling up an ASiCNR, in which the band gap increases with increasing tube diameter [24]. It is also noted that the lower conduction bands and the higher valence bands are twofold degeneration at Z point for broader 6- and 12-ASiCNRs as can be seen in Fig. 2e and f.

In order to study the variation of energy gap with ribbon width and chirality, the determined energy gaps as a function of ribbon width are summarized in Fig. 3 for (a) ZSiCNRs and (b) ASiCNRs with the ribbon width up to 20. Distinct variation behaviors are exhibited with increasing ribbon width between ZSiCNRs and ASiCNRs. For

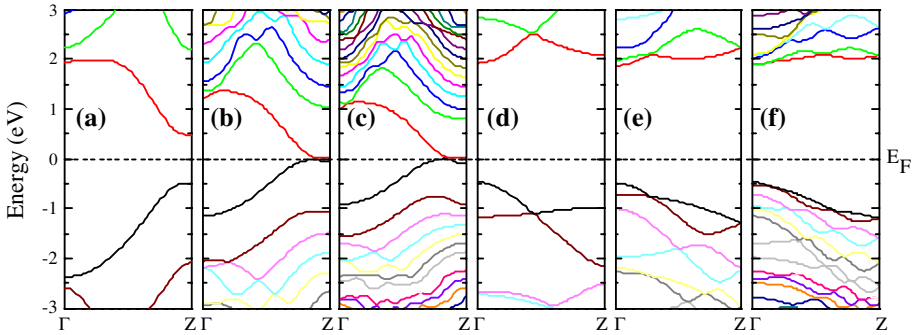

Fig. 2 The band structures for **a** 2-ZSiCNR, **b** 6-ZSiCNR, **c** 12-ZSiCNR, **d** 3-ASiCNR, **e** 6-ASiCNR, and **f** 12-ASiCNR. The Fermi level E_F is set to zero and is indicated by the horizontal *dashed lines*

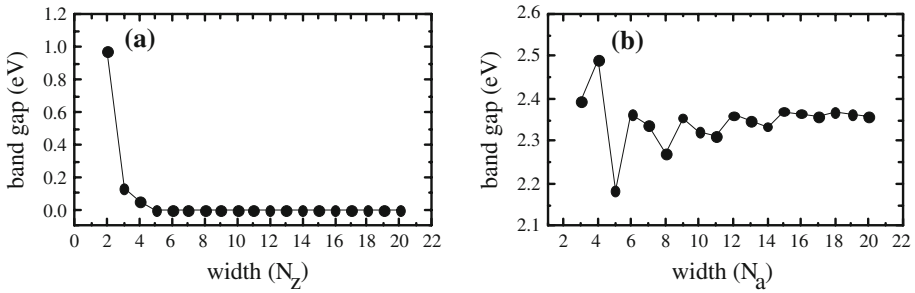

Fig. 3 Variation of energy band gap as a function of the width for **a** ZSiCNRs and **b** ASiCNRs

ZSiCNRs, the direct band gap decreases successively for the narrower $N_z = 2$, 3, and 4 and then becomes to zero after $N_z = 5$. This is because the bonding degree between free $\frac{1}{3}\pi$ electrons of the left edge C atom and free $\frac{1}{3}\pi$ electrons of the right edge Si atom without sharing with (or giving to) H atom and thus the direct band gap of semiconductor decreases for the narrower $N_z = 2$, 3, and 4 successively and then becomes to zero after $N_z = 5$. Though all the ASiCNRs are semiconductors regardless of their widths, the band gap oscillations are clearly seen with a significant quenching to a constant value of 2.359 eV as width of ASiCNR N_a increases. Such an oscillation behavior was also observed in AGNRs [10] and ABNNRs [13] only different constant values of 0 and 4.45 eV, respectively, were tended. In detail, except for the narrower $N_a = 3$, 4, and 5 due to strong interaction between two side edges, the band gap exhibits sawtooth-like periodic features with the highest and the lowest values corresponding to $N_a = 3n$ and $3n + 2$ ASiCNRs, respectively, for certain n ($n = 2$, 3, 4, 5, or 6). This is different from AGNRs and ABNNRs in which the highest and the lowest values corresponding to $N_a = 3n + 1$ and $3n + 2$.

The corresponding total density of states (DOS) (top panels) and projected density of states (PDOS) onto the C atom (middle panels) and Si atom (bottom panels) at edge (solid lines) and inner (dashed lines) sites are presented in Fig. 4 (a) 6-ZSiCNR, and (b) 6-ASiCNR as examples. It can be clearly seen in Fig. 4a for 6-ZSiCNR, that a sharp peak appears at the Fermi level E_F implying a metallic character. From the middle and bottom panels, one can further see that this sharp peak comes from the edge C atom (solid line) and edge Si atom (solid line). This is consistent with previous study for ZGNR [28]. Such a sharp peak does not appear at the Fermi level E_F in Fig. 4b for 6-ASiCNR as predicted from energy band structure of Fig. 2e. Secondly, it is interesting to note that for both 6-ZSiCNR and 6-ASiCNR, a driving down the DOS in lower energy region and a driving up the DOS in higher energy region for edge C or Si atoms (solid lines) with respect to the DOS of the inner C or Si atoms (dashed lines) below the Fermi level E_F. This is because the edge C or Si atoms have the fewer numbers of the near neighbors and thus the less restrictions coming from the near neighbor atoms, so the most electrons occupy higher energy states. Therefore, we conclude that the fewer coordination number will lead the most electrons to range in higher energy region of the occupancy state. Thirdly, the lower occupied valence bands are mainly localized to C atoms and the higher unoccupied conduction bands are mainly localized to Si atoms in Fig. 4a for 6-ZSiCNR as well as the HOVB and LUCB are highly localized to C and Si atoms, separately, in Fig. 4b for 6-ASiCNR. These are coincident with the charge distribution as shown in Fig. 5a and b that the valence charge density is strongly accumulated around C atoms due to their stronger 2p potential, and thus leads to a significant electron transfer from Si atoms to C atoms. The large asymmetry in charge distribution displays a typical ionic binding feature between Si and C atoms similar to III–V nanoribbons such as BNNRs [13] and AlNNRs [29]. In addition, Fig. 5a and b also shows that the C–H bond is covalent bond while Si–H bond is ionic bond.

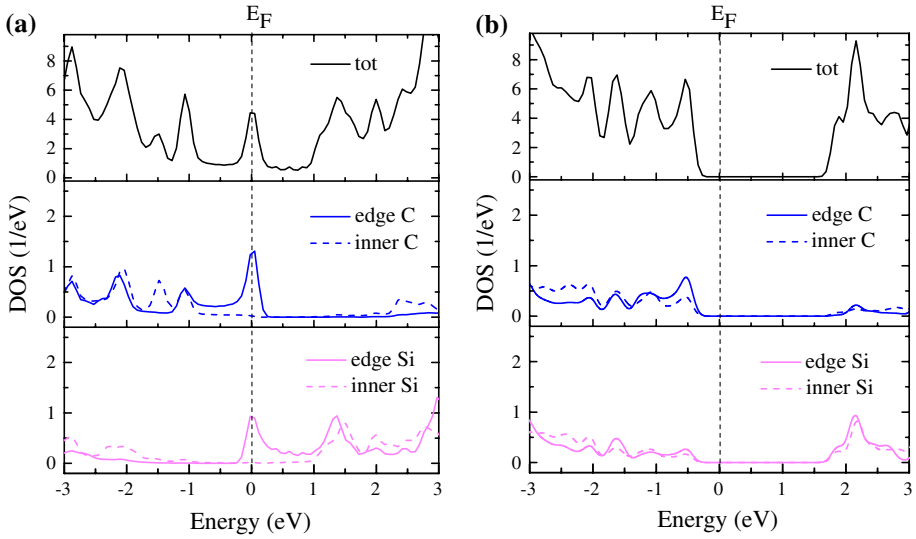

Fig. 4 The DOS for **a** 6-ZSiCNR and **b** 6-ASiCNR configuration. The top panels are the total DOS of the SiCNRs, the middle ones are the PDOS onto the edge (*solid line*) and inner (*dashed line*) C atoms, and the bottom ones are the PDOS onto the edge (*solid line*) and inner (*dashed line*) Si atoms. The Fermi level E_F is set to zero and is indicated by the vertical *dashed lines*

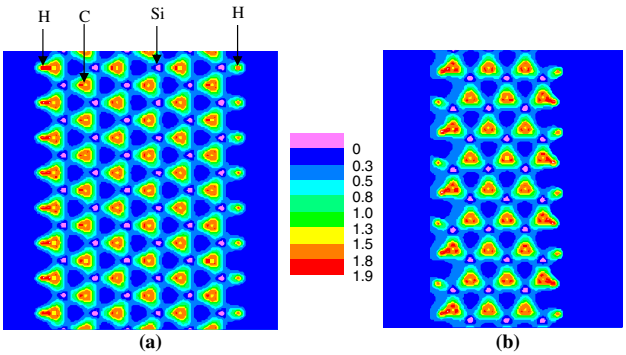

Fig. 5 The charge density contours of **a** 6-ZSiCNR and **b** 6-ASiCNR

As comparison studies, we also explore the effect of dangling bond on the electronic properties of SiCNRs. The band structures of 6-ZSiCNR with (a) bare C edge, (b) bare Si edge, and (c) bare C and Si edges as well as 6-ASiCNR with (d) bare C edge, (e) bare Si edge, and (f) bare C and Si edges are shown in Fig. 6. Comparing with Fig. 2b and e for the band structures of 6-ZSiCNR and 6-ASiCNR with H termination on both edges, one can readily see that the band structures are modified by dangling bonds. One (two) flat extra band (violet) appears at the Fermi level for 6-ZSiCNR with either bare C or bare Si edge (with bare C and Si edges) leading to the initial two met bands (red and black) separated from each other especially for bare Si edge (bare C and Si edges) accompanied with a up shift of the other bands with respect to them in Fig. 2b. For 6-ASiCNR without H termination, the bands still degenerate at Z point. A remarkable feature is that the two extra flat bands (violet) appear at the Fermi level as can be seen in Fig. 6 (d) bare C edge, and (e) bare Si edge. However, two nearly flat extra bands (violet) appear up and below the Fermi level for 6-ASiCNR with bare C and Si edges leading to an indirect band gap of 1.673 eV which is smaller than the direct band gap of 2.364 eV for 6-ASiCNR with H termination. This is consistent with the fact that many materials usually decrease the band gap when H termination is removed. In addition, the other bands shift up in Fig. 6d for bare C edge. The extra band is flat because it is originated from the dangling bond which is located at edge, as can be seen in Fig. 7 for projected density of states (PDOS) onto the edge C and/or Si atoms, and thus corresponds to a larger effective mass. We notice that in Fig. 6f for 6-ASiCNR with bare C and bare Si, a repulsion of extra bands (violet) is found instead of the appearance of them at the Fermi level as in the cases of bare C only and bare Si only in Fig. 6d and e, respectively. In order to check if such a band-repulsion found for the 6-ASiCNR is due to the limited width of the nanoribbon. A test with a wider nanoribbon, 12-ASiCNR for example, is further performed. The band structures of 12-ASiCNR with (g) bare C edge, (h) bare Si edge, and (i) bare C and Si edges are also shown in Fig. 6. Similar to 6-ASiCNR, two (nearly overlap) extra flat bands (violet) appear at the Fermi level in Fig. 6 (g) bare C edge and (h) bare Si edge. However, two (also nearly overlap) nearly flat extra bands (violet) appear up and below the Fermi level in Fig. 6 (i) for 12-ASiCNR with bare C and Si edges leading to an indirect band gap of 1.638 eV which is smaller than the direct band gap of 2.361 eV for 12-ASiCNR with H termination. That is, a repulsion of extra bands (violet) is also existed in 12-ASiCNR with bare C and Si edges. This implies that such a band-repulsion in ASiCNR with bare C and bare Si edges is width-independence.

The PDOS of 6-ZSiCNR, 6-ASiCNR, and 12-ASiCNR with bare C edge, bare Si edge, and bare C and Si edges are shown in Fig. 7. The blue and the light magenta lines are the PDOS onto edge C and Si atoms, respectively. The

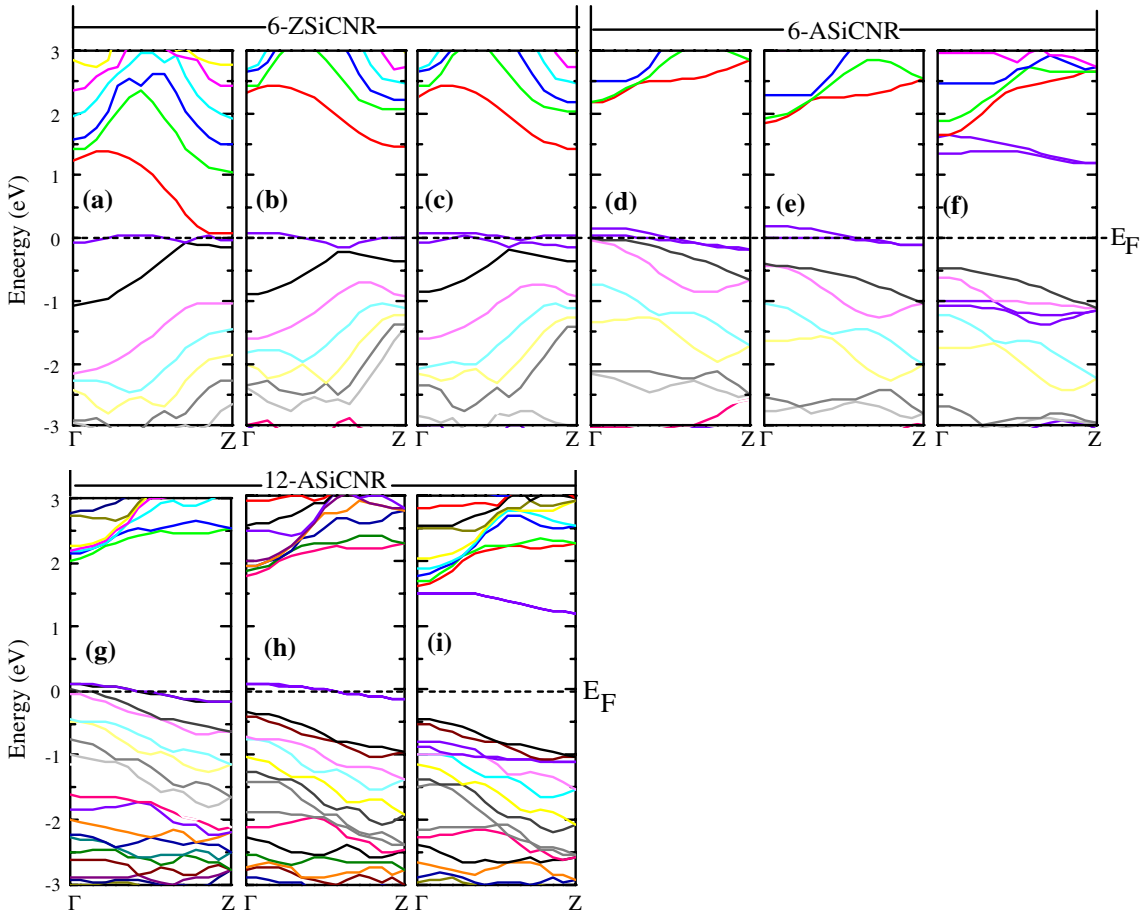

Fig. 6 The band structures of 6-ZSiCNR with **a** bare C edge, **b** bare Si edge, and **c** bare C and Si edges, 6-ASiCNR with **d** bare C edge, **e** bare Si edge, and **f** bare C and Si edges as well as 12-ASiCNR with **g** bare C edge, **h** bare Si edge, and **i** bare C and Si edges. The Fermi level E_F is set to zero and is indicated by the horizontal *dashed lines*

vertical dashed lines are Fermi level which is set to zero. We can see that for 6-ZSiCNR, the PDOS at the Fermi level E_F for bare C edge as well as bare C and Si edges ribbons are mainly come from the edge C atom while the PDOS at the Fermi level E_F for bare Si edge ribbon comes from edge C and Si atoms identically. Comparing relative values we know that the contributions from C atom are larger than that from the Si atom since some electrons have been transferred from Si to C. For 6-ASiCNR and 12-ASiCNR, the PDOS at the Fermi level for bare C and bare Si edges comes mainly from the edge C and Si atoms, respectively. Comparing with Fig. 7b for 6-ZSiCNR with bare Si edge also, in which the contributions to the PDOS at the Fermi level from edge Si atom are equal to that from edge C atom, one can see that in Fig. 7e and h for 6-ASiCNR and 12-ASiCNR with bare Si edge, the contributions to the PDOS at the Fermi level from edge Si atom are larger than that from edge C atom. This is because, as can be seen from Fig. 4a for 6-ZSiCNR with H termination, there is already a sharp peak at the Fermi level comes from the edge C atom (1.31) is larger than that from the edge Si atom (0.93). So in addition to the extra contribution from Si dangling bond an equal PDOS is obtained at the Fermi level for edge C and Si atoms. Such a sharp peak does not appear at the Fermi level in Fig. 4b for 6-ASiCNR with H termination. So in Fig. 7e and h for 6-ASiCNR and 12-ASiCNR with bare Si edge, the contributions to the PDOS at the Fermi level from edge Si atom is larger than that from edge C atom. As expected from the band structures in Fig. 6f and i, there is no PDOS at the Fermi level for bare C and Si edges, however, two extra peaks contributed from C and Si dangling bonds, respectively, appear at −1.1 and 1.4 eV in Fig. 7f for 6-ASiCNR with bare C and Si edges at −1.0 and 1.5 eV in Fig. 7i for 12-ASiCNR with bare C and Si edges, implying a strong interaction between dimer edge C and Si atoms from their partial electrons which are originally shared with (for edge C) or given to (for edge Si) the vanishing H termination. The higher

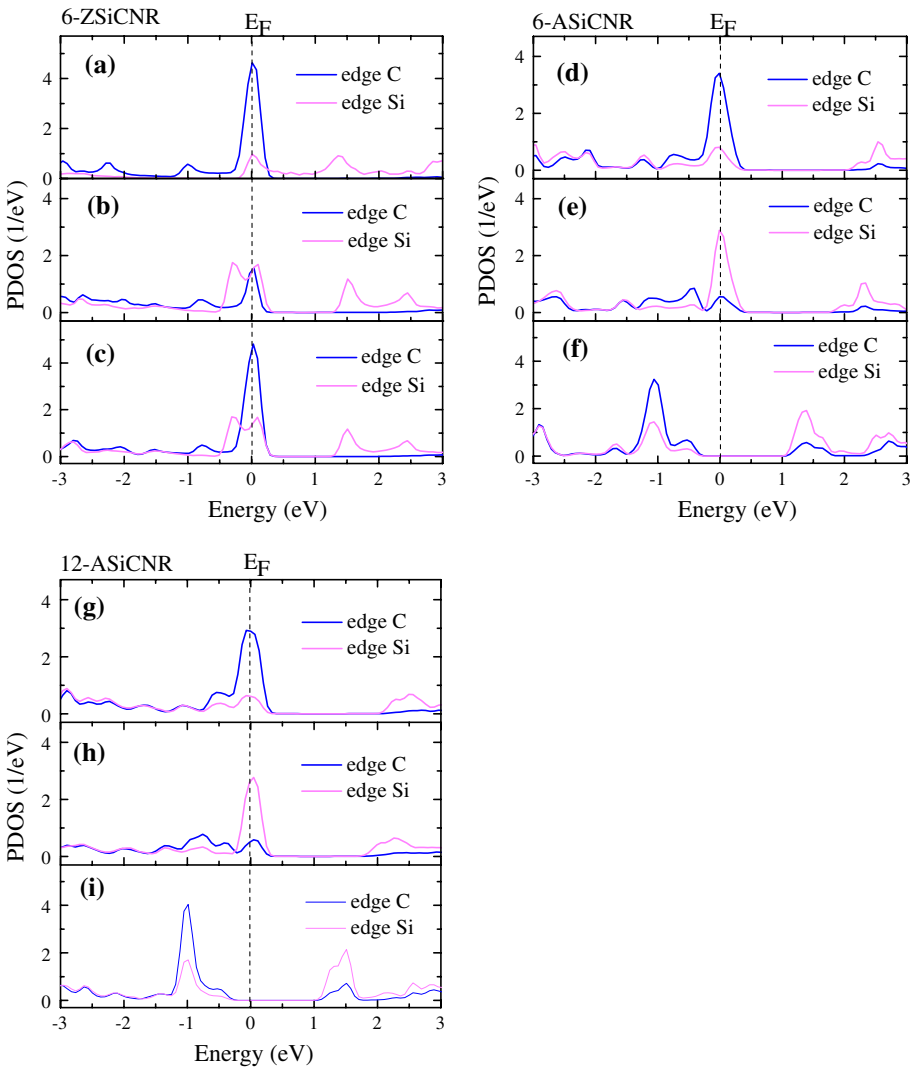

Fig. 7 The PDOS of 6-ZSiCNR with **a** bare Si edge, **b** bare C edge, and **c** bare Si and C edge, 6-ASiCNR with **d** bare C edge, **e** bare Si edge, and **f** bare Si and C edge as well as 12-ASiCNR with **g** bare C edge, **h** bare Si edge, and **i** bare Si and C edge. The *vertical dashed lines* are Fermi level which is set to zero

peak at −1.1 and −1.0 eV (occupied state) for edge C atom or the higher peak at 1.4 and 1.5 eV (unoccupied state) for edge Si atom also suggests the electrons transfer from Si atom to C atom even at edge without H termination.

Conclusions

In summary, the ZSiCNR and ASiCNR in width up to 20 have been investigated by using the first-principles PAW potential within the DFT framework under GGA. Distinct variation behaviors in band gap are exhibited with increasing ribbon width between ZSiCNRs and ASiCNRs. For ZSiCNRs, the direct band gap decreases successively for the narrower $N_z = 2$, 3, and 4 due to decreasing interaction between two side edges and then becomes to zero after $N_z = 5$. For ASiCNRs, except for the narrower $N_a = 3$, 4, and 5 due to strong interaction between two side edges, the band gap exhibits sawtooth-like periodic oscillation features with the highest and the lowest values corresponding to $N_a = 3n$ and $3n + 2$, respectively, and quenches to a constant value of 2.359 eV as width N_a increases.

The PDOS onto individual atom shows that a sharp peak appeared at the Fermi level for 6-ZSiCNR as an example comes from the edge C and Si atoms with H terminations. But such a sharp peak does not appear for 6-ASiCNR.

The charge density contours analysis shows the valence charge is strongly accumulated around C atoms due to their stronger 2p potential, and thus leads to a significant electron transfer from Si atoms to C atoms and a typical ionic binding feature similar to III–V nanoribbons. In addition, the Si–H bond is also ionic bond while the C–H bond is covalent bond.

The band structures are modified by dangling bonds. One (two) flat extra band appears at the Fermi level for 6-ZSiCNR with either bare C or bare Si edge (with bare C

and Si edges). While two extra flat bands appear at the Fermi level for 6-ASiCNR and 12-ASiCNR with either bare C edge or bare Si edge, and two nearly flat extra bands appear up and below the Fermi level for 6-ASiCNR and 12-ASiCNR with bare C and Si edges.

Acknowledgements The authors would like to acknowledge the State Key Development for Basic Research of China (Grant No. 2004CB619302) for providing financial support for this research.

References

1. Novoselov KS, Geim AK, Morozov SV, Jiang D, Zhang Y, Dubonos SV, Grigorieva IV, Filrsov AA (2004) Science 306:666
2. Geim AK, Novoselov KS (2007) Nature Mater 6:183
3. Novoselov KS, Geim AK, Morozov SV, Jiang D, Katsnelson MI, Grigorieva IV, Dubonos SV, Firsov AA (2005) Nature 438:197
4. Zhang Y, Tan YW, Stormer HL, Kim P (2005) Nature 438:201
5. Berger C, Song ZM, Li XB, Wu XS, Brown N, Naud C, Mayou D, Li TB, Hass J, Marchenkov AN, Conrad EH, First PN, de Heer WA (2006) Science 312:1191
6. Nakada K, Fujita M (1996) Phys Rev B 54:17954
7. Miyamoto Y, Nakada K, Fujita M (1999) Phys Rev B 59:9858
8. Kawai T, Miyamoto Y, Sugino O, Koga Y (2000) Phys Rev B 62 R:16349
9. Ezawa M (2006) Phys Rev B 73:045432
10. Son YW, Cohen ML, Louie SG (2006) Phys Rev Lett 97:216803
11. Harris GL (1995) Properties of silicon carbide. INSPEC, London
12. Wakabayashi K, Fujita M, Ajiki H, Sigrist M (1999) Phys Rev B 59:8271
13. Du AJ, Smith SC, Lu GQ (2007) Chem Phys Lett 447:181
14. Kresse G, Hafner J (1993) Phys Rev B 47:558
15. Kresse G, Hafner J (1994) Phys Rev B 49:14251
16. Kresse G, Furthmüller J (1996) Comput Mater Sci 6:15
17. Kresse G, Furthmüller J (1996) Phys Rev B 54:11169
18. Blügel S (1988) PhD Thesis, RWTH Aachen
19. Johnson DD (1988) Phys Rev B 38:12087
20. Pulay P (1980) Chem Phys Lett 73:393
21. Kresse G, Joubert D (1999) Phys Rev B 59:1758
22. Perdew JP, Burke K, Ernzerhof M (1996) Phys Rev Lett 77:3865
23. Monkhorst HJ, Pack JD (1976) Phys Rev B 13:5188
24. Zhao MW, Xia YY, Li F, Zhang RQ, Lee S-T (2005) Phys Rev B 71:085312
25. Menon M, Richter E, Mavrandonakis A, Froudakis G, Andriotis AN (2004) Phys Rev B 69:115322
26. Mavrandonakis A, Froudakis GE, Schnell M, Muhlhăuser M (2003) Nano Lett 3:1481
27. Zhao MW, Xia YY, Zhang RQ, Lee S-T (2005) J Chem Soc 122:214707
28. Yu SS, Zheng WT, Wen QB, Jiang Q (2008) Carbon 46:537
29. Du AJ, Zhu ZH, Chen Y, Lu GQ, Smith SC (2009) Chem Phys Lett 469:183